Journal of Hydraulic Research

ISSN: (Print) (Online) Journal homepage: https://www.tandfonline.com/loi/tjhr20

Gravity currents from a constant inflow on unbounded uniform slopes

Ching-Sen Wu & Albert Dai

To cite this article: Ching-Sen Wu & Albert Dai (2023) Gravity currents from a constant inflow on unbounded uniform slopes, Journal of Hydraulic Research, 61:6, 880-892, DOI: 10.1080/00221686.2023.2267511

To link to this article: https://doi.org/10.1080/00221686.2023.2267511

Journal of Hydraulic Research Vol. 61, No. 6 (2023), pp. 880–892
https://doi.org/10.1080/00221686.2023.2267511

Research paper

Gravity currents from a constant inflow on unbounded uniform slopes

CHING-SEN WU, Associate Professor, *Department of Civil Engineering, National Ilan University, Yilan, Taiwan, ROC*
Email: olivercswu@niu.edu.tw

ALBERT DAI, Professor, *Department of Engineering Science and Ocean Engineering, National Taiwan University, Taipei, Taiwan, ROC*
Email: hdai@ntu.edu.tw (author for correspondence)

ABSTRACT
In this study we conducted laboratory experiments to examine the gravity currents produced from a constant inflow propagating on unbounded uniform slopes in the range $0^\circ \leq \theta \leq 15^\circ$. In the experiments, the inlet Reynolds number and the slope angle were varied systematically. The study carried out dimensional analysis and quantified five dimensionless parameters, thereby characterizing the development of gravity currents. Top-view images shown in the experiments exhibited gravity currents in an elongated shape when propagating on steeper slopes larger than 6° but a round shape on milder slopes less than 3°. The study finds that the five dimensionless parameters, which are functions of the slope angle, have near constant values for sufficiently large inlet Reynolds number, suggesting that the flow is approaching the regime of Reynolds number independence. The results from our experiments are expected to be applicable to gravity currents produced from a constant inflow on unbounded uniform slopes in larger scale natural or man-made environments.

Keywords: Constant inflow; dimensional analysis; gravity currents; inclined bottom; laboratory experiments

1 Introduction

Gravity currents, or density currents, are buoyancy-driven flows often in the horizontal direction that occur upon intrusion of one fluid into another with a different density (Huppert, 2006), due to difference in salinity, temperature and concentration of suspended particles or their combination. Gravity currents take place in both nature and man-made environments, such as overflow in river channels or estuaries and powder-snow avalanches (Allen, 1985; Fannelop, 1994; Simpson, 1997). Previous studies have mostly focused on gravity currents produced from the release of a finite buoyancy source and propagating on a horizontal bottom in channels with lateral confining walls, in lock-exchange experiments, in which such currents exhibit a distinct head and a tail (Adduce et al., 2012; Borden & Meiburg, 2013; Cantero et al., 2007; Huppert & Simpson, 1980; La Rocca et al., 2008; Maggi et al., 2022; Marino et al., 2005; Nogueira et al., 2013a, 2013b; Shin et al., 2004; Ungarish, 2009; Ungarish & Hogg, 2018; Wu & Dai, 2020). Gravity current propagating over an inclined bottom is also a common natural phenomenon, such as in powder-snow avalanches (Hopfinger, 1983), spillage of hazardous materials (Fannelop, 1994), turbidity currents in submarine canyons and saline undercurrents in estuaries (Simpson, 1997). In laboratory experiments, gravity current propagating on a slope can be produced by releasing a finite volume of heavy fluid in a channel with lateral walls (Dai, 2013a, 2013b, 2014; Dai & Garcia, 2010; Dai et al., 2012; Martin et al., 2019; Negretti et al., 2017) or on an unbounded uniform slope (Dai & Huang, 2020, 2021; Ross et al., 2002). Likewise, gravity currents produced from a continuous inflow of heavy fluid can occur in a channel with lateral walls (Baines, 2001; Britter & Linden, 1980) or on an unbounded uniform slope (Alavian, 1986; Bonnecaze & Lister, 1999; Hauenstein & Dracos, 1984). This study aimed at investigating gravity currents produced from a constant inflow, which propagate on different unbounded uniform slopes. Gravity currents in such a configuration tended to develop a three-dimensional pattern, with their width and the height of their heads increasing in the streamwise direction, an area scantly covered by previous studies, to the best of our knowledge. Some studies have conducted quasi-analytical, experimental, or numerical investigations of the problem, as outlined next.

Hauenstein and Dracos (1984) proposed a model containing momentum-dominated constant inflow of heavy fluid, plunging

Received 11 February 2023; accepted 29 September 2023/Currently open for discussion.

ISSN 0022-1686 print/ISSN 1814-2079 online
http://www.tandfonline.com

of inflow, and resulting buoyancy-dominated three-dimensional gravity currents. They observed that the gravity currents in the buoyancy-dominated region consist of a steady part, which is the body of the currents, and an unsteady part, capping the currents. The unsteady cap was assumed to be fed with mass, momentum and buoyancy at its centre. In the model, while some parameters have to be determined experimentally, its coefficients are functions of the parameters measured in experiments. Based on the experimental data, two relationships were proposed as follows:

$$b_{\max} = \frac{\cos\theta}{C_6} x_{f,v} \quad \text{and} \quad b_{\max} = 1.11 W_p^{1/4} t^{3/4} \tag{1}$$

where $x_{f,v}$ is the front location in the streamwise direction measured from virtual origin, $b_{\max}$ the maximum width of the current in the spanwise direction, W_p the buoyancy flux, C_6 an empirical constant associated with the relative density difference between the inflow and ambient fluid, $\Delta\rho/\rho_0$:

$$C_6 = \cos\theta \left(1 + 40\frac{\Delta\rho}{\rho_0}\right) \tag{2}$$

Martin et al. (2019) and Negretti et al. (2017) looked into flow morphologies on continuously supplied gravity currents from a horizontal direction to sloping, with straight or concave boundary. Chawdhary et al. (2018) conducted a numerical investigation of the flow dynamics of gravity currents with coherent structure on two slopes of 5° and 15° in a laboratory-scale tank.

The study attempted to examine the gravity currents produced from a constant inflow which propagate on unbounded uniform slopes, finding preliminarily that the model proposed by Hauenstein and Dracos (1984) could be applied to experimental data only at a limited scale, as its coefficients may take unphysical values. Therefore, the study looked into the characteristics of gravity currents produced from a constant inflow on unbounded uniform slopes and attempted to find similarities of gravity currents so that the results can be applied to situations at larger scale. With the density difference between the inflow heavy fluid and light ambient fluid maintained unchanged, the inlet Reynolds number, defined as $\mathsf{Re} = (Q_0 h_0^{-1})/\nu$ and controlled by volumetric inflow rate Q_0, and the slope angle θ are varied systematically in the experiments, where the lock height of release h_0 and fluid kinematic viscosity ν are unchanged. In the experiments, the dimension of the lock height of release has influence on the flow velocity out of the lock. The study focused on investigating the buoyancy-dominated flow regime reaching a quasi-steady state. With h_0 being kept at a smaller value while the inflow rate maintained unchanged, the flow velocity would increase such that the gravity currents become momentum-dominated. To capture the gravity currents in the buoyancy-dominated regime reaching a quasi-steady state without expanding the flume's dimensions, h_0 is chosen at a sufficiently large value and maintained a constant in the experiments. The study looked into the measurement of the dimensionless parameters of gravity currents, under the influence of inflow rate and slope angle. The following is an exhibition of gravity currents produced from a constant volumetric inflow in the range of 0.6–3.61 min^{-1} (or equivalently 10–60 $\mathrm{cm}^{-3}\,\mathrm{s}^{-1}$ in SI unit) and at slope angles $\theta = 15°, 12°, 9°, 6°, 3°, 0°$. The remainder of the paper is organized as follows: Section 2, dimensional analysis of gravity currents; Section 3, experimental apparatus and techniques; Section 4, qualitative observation based on experimental images and quantitative measurement based on dimensional analysis; and finally, Section 5, conclusions.

2 Theoretical approach

A sketch of the problem is shown in Fig. 1, in which ρ_1 represents the density of heavy fluid and ρ_0 represents the density of ambient fluid. The heavy fluid flows into the environment through an inlet with a cross-sectional area $b_0 h_0$. Assuming a small density difference, $\Delta\rho/\rho_0 < 5\%$, the gravity currents can be classified as Boussinesq (Dai, 2014; Dai & Huang, 2021; Maxworthy, 2010). For the sake of convenience, most nomenclatures follow Hauenstein and Dracos (1984). Upon the release of heavy fluid from the inlet, gravity currents propagate in the streamwise direction and spread in the spanwise direction, taking shape during the propagation process, including maximum width $b_{\max}$, maximum head height h, front location x_f, head density $\Delta\rho_f$, and time dependence t. Variables are included in the following function form:

$$x_f = f\,(h, Q_0, g', b_{\max}, \Delta\rho, \Delta\rho_f, \theta, t) \tag{3}$$

With the density difference between the inflow heavy fluid and light ambient fluid being maintained unchanged, the volumetric inflow rate can be considered, along with reduced gravity $g' \equiv (\Delta\rho/\rho_0)g$, as the buoyancy flux $W_p \equiv Q_0 g'$. The dimension of the lock height of release remained constant in the experiments for the gravity currents in the buoyancy-dominated flow regime. The front location (x_f) and the inflow buoyancy flux (W_p) were chosen as repeating variables and consequently the problem was subject to the influence of the inlet Reynolds number Re and the slope angle θ. With the density difference between the inflow heavy fluid and light ambient fluid being maintained unchanged, the inflow buoyancy flux and the inlet Reynolds number were both under the control of the volumetric inflow Q_0.

In investigating the gravity currents, the aforementioned quantities of interest can be expressed in a function form of dimensionless parameters. Based on the Buckingham-π theorem, five dimensionless parameters of greatest interest can be specified. First, dimensionless parameters π_1 and π_2 represent, respectively, shape factors for the expansion of gravity currents in the spanwise direction and expansion of gravity current in the wall-normal direction:

$$\pi_1 = b_{\max}/x_f \tag{4}$$

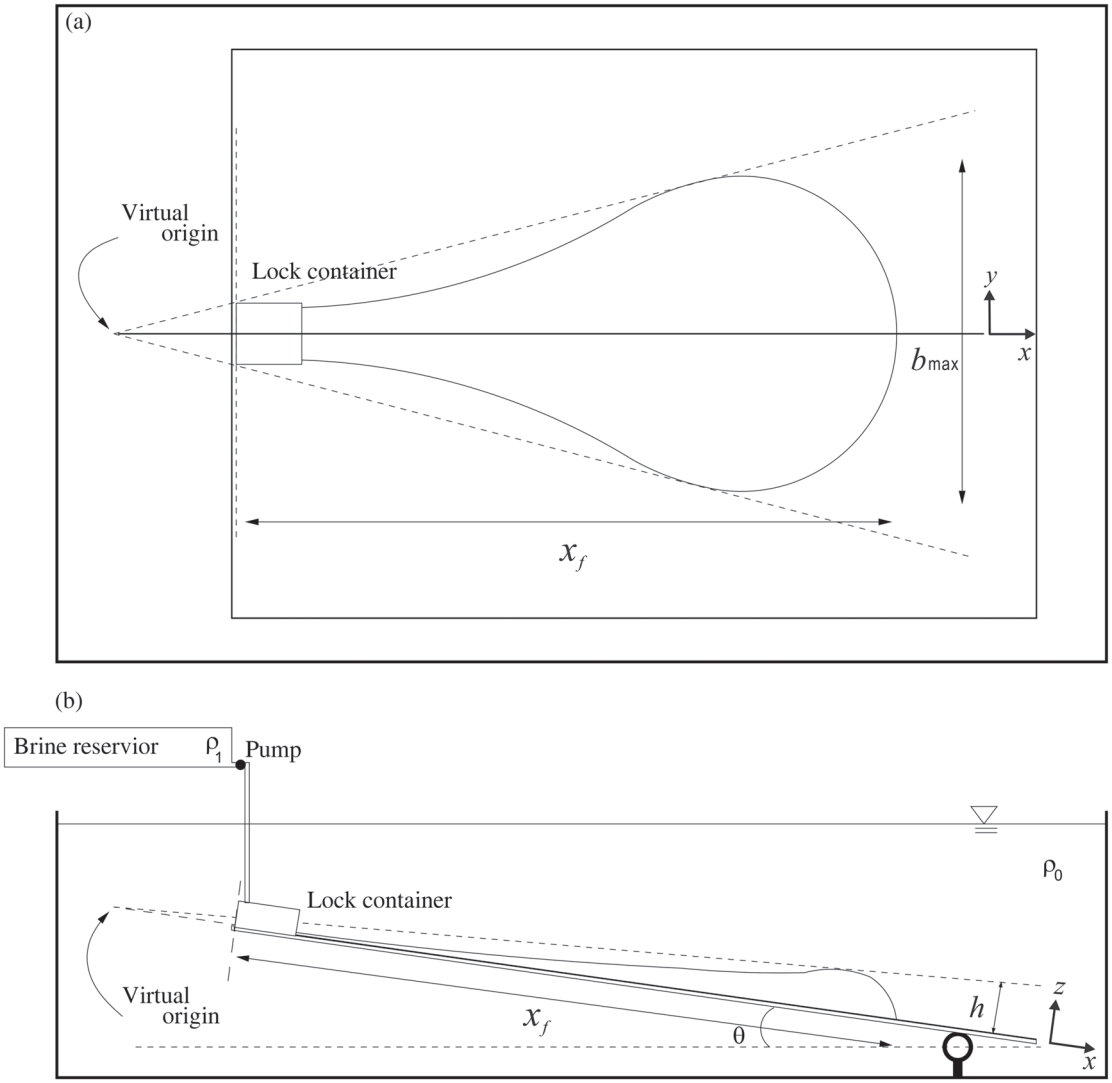

Figure 1 Sketch of experimental set-up of the study on gravity currents propagating on unbounded uniform slopes with angle θ to the horizontal, as viewed from the top (a) and side (b). Fresh water with density ρ_0 was used as ambient fluid, while heavy fluid is salt water with density ρ_1. x_f is the distance of the gravity current front, measured in a lock container

$$\pi_2 = h/x_f \tag{5}$$

where h represents the measured maximum height of current head at each instant increasing along with the propagating current front x_f from side-view experimental images. Parameters π_3 and π_4 represent, respectively, the relationship between the front location and time and the relationship between the maximum width and time:

$$\pi_3 = x_f^{-4/3} {W_p}^{1/3} t, \tag{6}$$

$$\pi_4 = b_{\max}^{4/3} {W_p}^{-1/3} t. \tag{7}$$

Dimensionless parameter π_5 represents the variation of the density of fluid in the head, which can be expressed as:

$$\pi_5 = x_f^{5/3} {W_p}^{-2/3} \left(\frac{\Delta\rho_f}{\rho_0} g \right) \tag{8}$$

in which $\Delta\rho_f$ represents the density of fluid in the head. The dimensionless parameters π_1, π_2, π_3, π_4, π_5 are functions of the slope angle θ and the inlet Reynolds number Re.

3 Experimental set-up

The study employed a rectangular tank 2.8 m long, 1.85 m wide, and 0.85 m high, as shown in Fig. 1, made of transparent Perspex board. A Perspex board 2.47 m long and around 1.6 m wide was installed at the bottom of the tank serving as the inclined boundary at an angle ranging $0^\circ \leq \theta \leq 15^\circ$ in the experiments. The tank was initially filled with tap water. We used salt water as the heavy fluid which was coloured by potassium permanganate for flow visualization. Heavy fluid was pumped through a plastic tube into a diffuser 9 cm long, 8.5 cm wide, and 3 cm high, mounted on the top of the slope. Inflowing heavy fluid passed through a mesh grid in the front of the diffuser, which

Table 1 Operational parameters for gravity currents produced from a constant inflow on unbounded uniform slopes

Experiment	θ	Q_0 ($\mathrm{cm^3\,s^{-1}}$)	ρ_1 ($\mathrm{g\,cm^{-3}}$)	ρ_0 ($\mathrm{g\,cm^{-3}}$)	$\Delta\rho g/\rho_0$ ($\mathrm{cm\,s^{-2}}$)	Re
A1	0°	10 ± 0.33	1.0484 ± 0.0001	0.9965 ± 0.0001	51.09 ± 0.51	303.0
A2	0°	20 ± 0.67	1.0484 ± 0.0001	0.9963 ± 0.0001	51.30 ± 0.51	606.1
A3	0°	40 ± 1.33	1.0484 ± 0.0001	0.9962 ± 0.0001	51.40 ± 0.51	1212.1
A4	0°	60 ± 2.00	1.0484 ± 0.0001	0.9963 ± 0.0001	51.29 ± 0.51	1818.2
B1	3°	10 ± 0.33	1.0480 ± 0.0001	0.9962 ± 0.0001	51.01 ± 0.51	303.0
B2	3°	20 ± 0.67	1.0480 ± 0.0001	0.9963 ± 0.0001	50.91 ± 0.51	606.1
B3	3°	40 ± 1.33	1.0480 ± 0.0001	0.9963 ± 0.0001	50.91 ± 0.51	1212.1
B4	3°	60 ± 2.00	1.0480 ± 0.0001	0.9963 ± 0.0001	50.91 ± 0.51	1818.2
C1	6°	10 ± 0.33	1.0481 ± 0.0001	0.9963 ± 0.0001	51.00 ± 0.51	303.0
C2	6°	20 ± 0.67	1.0481 ± 0.0001	0.9962 ± 0.0001	51.11 ± 0.51	606.1
C3	6°	40 ± 1.33	1.0481 ± 0.0001	0.9963 ± 0.0001	51.00 ± 0.51	1212.1
C4	6°	60 ± 2.00	1.0481 ± 0.0001	0.9965 ± 0.0001	50.80 ± 0.51	1818.2
D1	9°	10 ± 0.33	1.0489 ± 0.0001	0.9971 ± 0.0001	50.96 ± 0.51	303.0
D2	9°	20 ± 0.67	1.0489 ± 0.0001	0.9969 ± 0.0001	51.17 ± 0.51	606.1
D3	9°	40 ± 1.33	1.0489 ± 0.0001	0.9966 ± 0.0001	51.48 ± 0.51	1212.1
D4	9°	60 ± 2.00	1.0489 ± 0.0001	0.9970 ± 0.0001	51.07 ± 0.51	1818.2
E1	12°	10 ± 0.33	1.0486 ± 0.0001	0.9968 ± 0.0001	50.98 ± 0.51	303.0
E2	12°	20 ± 0.67	1.0486 ± 0.0001	0.9966 ± 0.0001	51.19 ± 0.51	606.1
E3	12°	40 ± 1.33	1.0486 ± 0.0001	0.9967 ± 0.0001	51.08 ± 0.51	1212.1
E4	12°	60 ± 2.00	1.0486 ± 0.0001	0.9967 ± 0.0001	51.08 ± 0.51	1818.2
F1	15°	10 ± 0.33	1.0482 ± 0.0001	0.9963 ± 0.0001	51.10 ± 0.51	303.0
F2	15°	20 ± 0.67	1.0482 ± 0.0001	0.9964 ± 0.0001	51.00 ± 0.51	606.1
F3	15°	40 ± 1.33	1.0482 ± 0.0001	0.9963 ± 0.0001	51.10 ± 0.51	1212.1
F4	15°	60 ± 2.00	1.0482 ± 0.0001	0.9964 ± 0.0001	51.00 ± 0.51	1818.2

Note: At least three repetitive runs were conducted for each experimental set-up. The inlet Reynolds number, Re, is defined as $\mathsf{Re} = (Q_0 h_0^{-1})/\nu$, in which ν is the kinematic viscosity.

was fully submerged, with excess air being removed manually before running the experiments.

A Canon EOS 700D Digital SLR (Tokyo, Japan) and a Sony HDR-PJ670 video were employed to capture flow images, up to 1920×1080 pixels full HD resolutions (Tokyo, Japan) at 24 frames per second, which were transferred to a PC for processing. The two cameras were placed on the side and top of the tank, respectively, and adjusted, so that the horizontal and vertical axes in the side-view images align with the inclined boundary and wall-normal directions.

Two LED light boards with light-diffusing screen were placed on the sidewalls of the tank, providing uniform illumination. Densities of inflowing heavy fluid and light ambient fluid were around $\rho_1 \approx 1.048\,\mathrm{g\,cm^{-3}}$ and $\rho_0 \approx 0.9965\,\mathrm{g\,cm^{-3}}$, respectively. Operating parameters in each experiment were listed in detail in Table 1. Fluid density was measured with a density meter with an accuracy of $10^{-4}\,\mathrm{g\,cm^{-3}}$. The kinematic viscosity of the saline mixture is taken as $\nu = 1.1 \times 10^{-2}\,\mathrm{cm^2\,s^{-1}}$. Fluid samples from various downstream sites were collected with a syringe for density measurement. Six fixed probes were installed in the streamwise direction. Samples were taken immediately when the current front reached the tip of the needle.

With the density difference between the inflow heavy fluid and light ambient fluid being maintained unchanged, the inlet Reynolds number, controlled by volumetric inflow rate Q_0, and the slope angle θ, were varied systematically in the experiments. The volumetric inflow rate was in the range of 0.6–$3.6\,\mathrm{l\,min^{-1}}$ (or equivalently 10–$60\,\mathrm{cm^{-3}\,s^{-1}}$ in SI units) and the slope angle in the range of $0° \le \theta \le 15°$. A total of 24 experiments with three repeated runs each were carried out in the study.

4 Results

In this study we presented two qualitatively different types of gravity currents propagating on unbounded uniform slopes, one on steeper slopes $\theta = 15°, 12°, 9°, 6°$ and the other on milder slopes $\theta = 3°$, $0°$. There were four inlet Reynolds numbers, $\mathsf{Re} = (Q_0 h_0^{-1})/\nu$, corresponding to volumetric inflow rates $Q_0 = 0.6, 1.2, 2.4, 3.6\,\mathrm{l\,min^{-1}}$. Two types of flow morphologies were classified via qualitative observation and quantitative measurement was done via dimensional analysis.

4.1 *Gravity currents on steeper slopes* $\theta = 15°, 12°, 9°$ *and* $6°$

Figures 2 and 3 show the instantaneous images of gravity currents propagating on unbounded uniform slopes at $\theta \ge 6°$. Figure 2 shows the gravity currents propagating in the downslope direction at the minimum volumetric flow rate, $Q_0 = 0.6\,\mathrm{l\,min^{-1}}$, in contrast to the maximum volumetric flow rate, $Q_0 = 3.6\,\mathrm{l\,min^{-1}}$ as shown in Fig. 3. At the minimum inflow

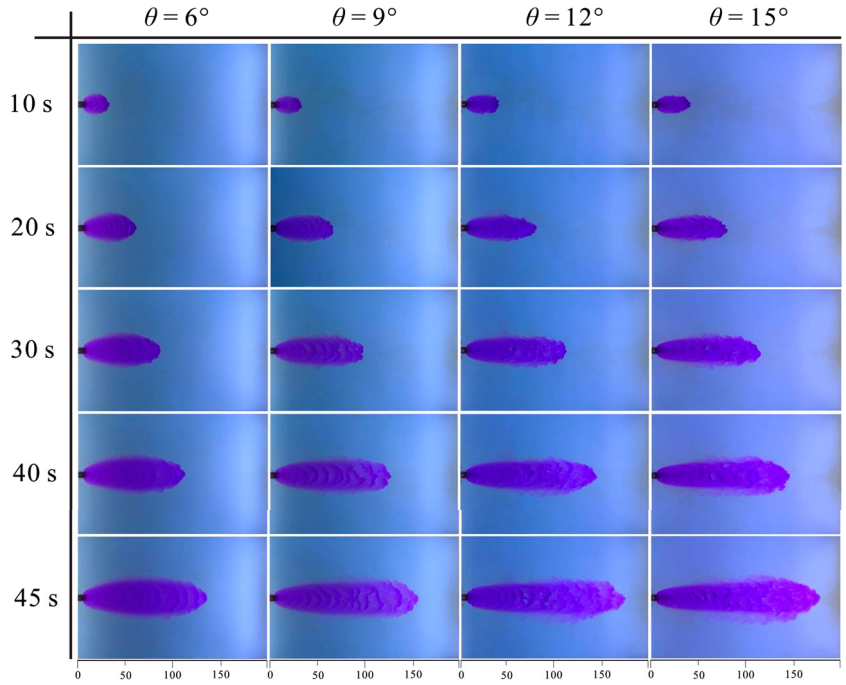

Figure 2 Flow images of gravity currents produced from a constant inflow which propagate on slopes at volumetric flow rate $Q_0 = 0.6\,\mathrm{l\,min^{-1}}$ (equivalent to $10\,\mathrm{cm^3\,s^{-1}}$). The rows, from top to bottom, refer to time instances at $t = 10$, 20, 30, 40, 45 s, while the images from left to right columns refer to gravity currents on $\theta = 6°$, 9°, 12° and 15°, respectively

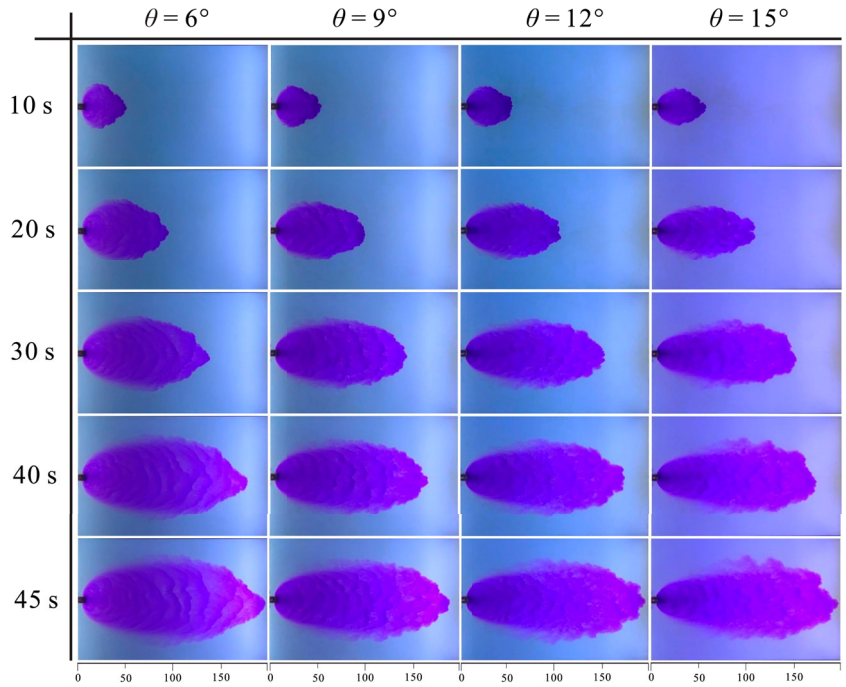

Figure 3 Flow images of gravity currents produced from a constant inflow which propagate on slopes at volumetric flow rate $Q_0 = 3.6\,\mathrm{l\,min^{-1}}$ (equivalent to $60\,\mathrm{cm^3\,s^{-1}}$). The images from left to right columns refer to gravity currents on $\theta = 6°$, 9°, 12° and 15°, respectively

rate, the width of currents varied slowly in an elongated shape and the current head was rather round initially as $t \leq 10$ s. Afterwards, the expansion of gravity currents in the lateral direction slowed down as slope angle increased. At the maximum inflow rate, the gravity currents propagate downslope in an elongated shape. As shown in Figs 2 and 3, the spreading of gravity currents in the lateral direction was a function of the inlet buoyancy flux and slope angle, so was the thickness of current head, as shown in Figs 4 and 5.

As shown in the flow images in Figs 2 and 3, the front location can be pinpointed definitely, exhibiting the foremost downstream location of gravity currents. No further calibration was required to ascertain the position of the front (Adduce et al., 2022). The front velocity can be calculated from the

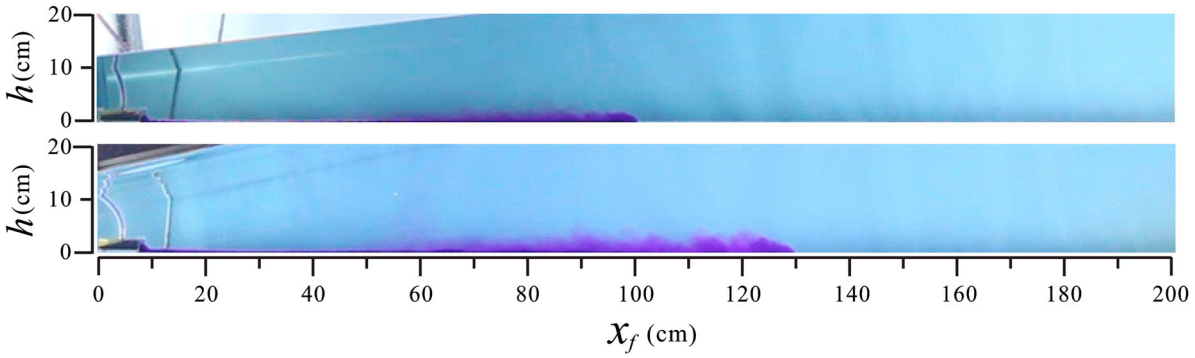

Figure 4 Side-view flow images of gravity currents produced from a constant inflow at volumetric flow rate $Q_0 = 0.6\,\mathrm{l\,min^{-1}}$ (or equivalently $10\,\mathrm{cm^3\,s^{-1}}$) on 6° slope (top) and on 12° slope (bottom). Distances in the streamwise and wall-normal directions are in units of cm, with time instances set at $t = 30\,\mathrm{s}$

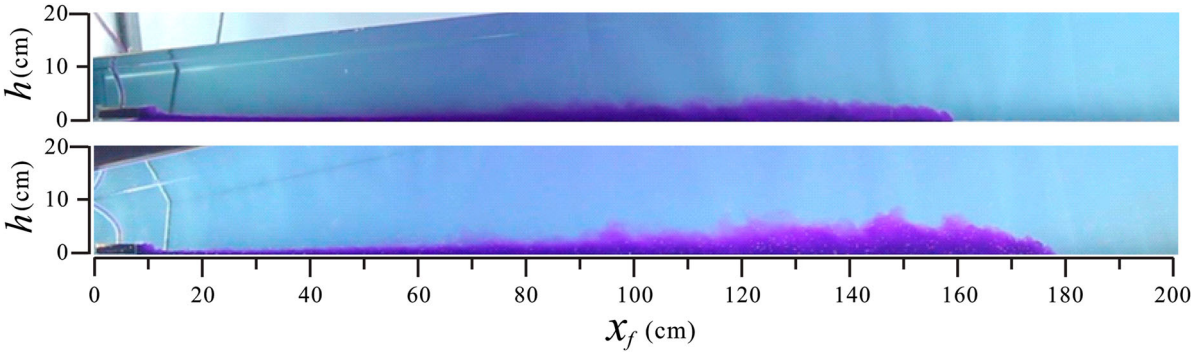

Figure 5 Side-view flow images of gravity currents produced from a constant inflow at volumetric flow rate $Q_0 = 3.6\,\mathrm{l\,min^{-1}}$ (or equivalently $60\,\mathrm{cm^3\,s^{-1}}$) on 6° slope (top) and on 12° slope (bottom). Distances in the streamwise and wall-normal directions are in units of cm, with time instances set at $t = 30\,\mathrm{s}$

time rate of change of the front location. Figure 6 shows the front velocity histories for $\theta = 6^\circ$ and $\theta = 12^\circ$, indicating that after the heavy fluid flowing out of the diffuser, the front velocity reached a peak value before decelerating. In Fig. 6a, the front velocity decelerates gradually while demonstrating transient oscillations after reaching the peak front velocity. In contrast, in Fig. 6b, when the gravity currents propagate on a 6° slope, the front velocity decreases more smoothly. It is inferred that the transient oscillations in the front velocity occur when the heavy fluid in the body of the current flowing down a steeper slope, at a somewhat higher speed, overruns the advancing front.

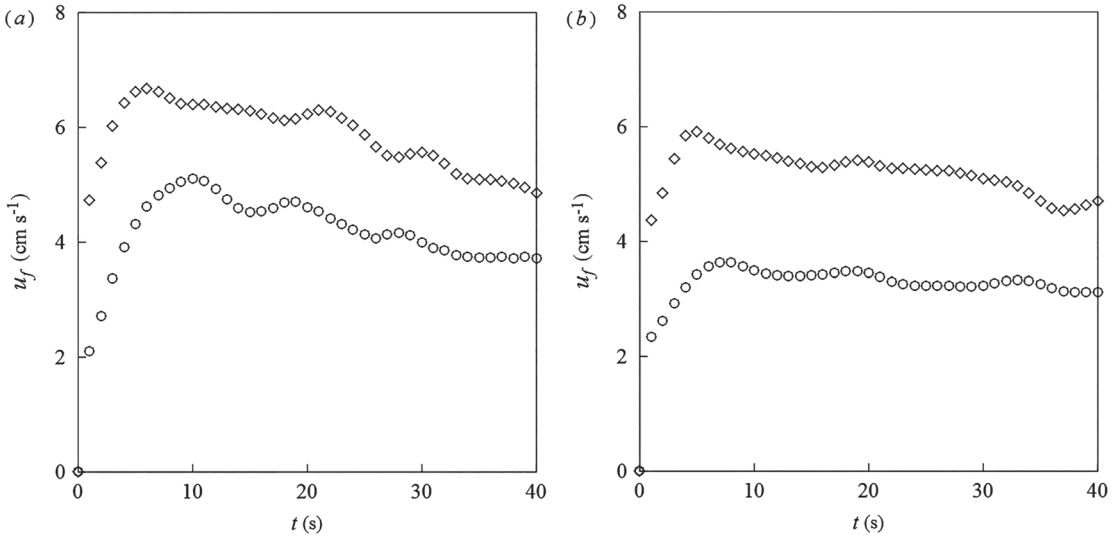

Figure 6 Front velocity histories for the gravity currents produced from constant inflow rates, $Q_0 = 0.6\,\mathrm{l\,min^{-1}}$ (equivalent to $10\,\mathrm{cm^3\,s^{-1}}$) (°) and $3.6\,\mathrm{l\,min^{-1}}$ (equivalent to $60\,\mathrm{cm^3\,s^{-1}}$) (◇) on unbounded uniform slopes; (a) $\theta = 12^\circ$ and (b) $\theta = 6^\circ$

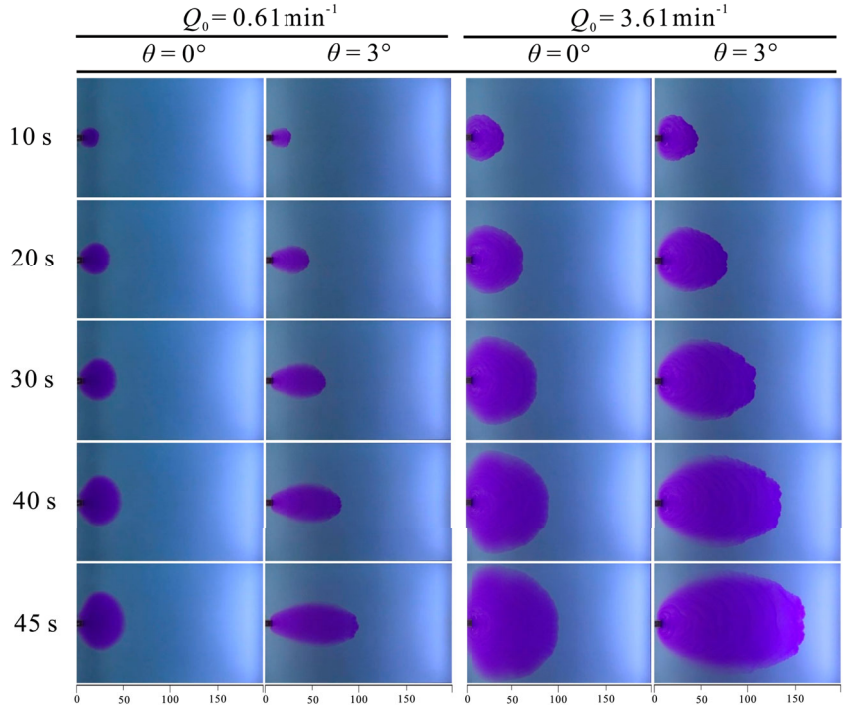

Figure 7 Flow images for gravity currents produced from constant inflow rates which propagate on a 3° slope and on the horizontal boundary at $Q_0 = 0.6\,\mathrm{l\,min^{-1}}$ and $3.6\,\mathrm{l\,min^{-1}}$ (equivalent to $10\,\mathrm{cm^3\,s^{-1}}$ and $60\,\mathrm{cm^3\,s^{-1}}$). The rows from top to bottom refer to time instances at $t = 10$, 20, 30, 40, 45 s, which images from left to right columns refer to the gravity currents on $\theta = 0°$, 3°, respectively

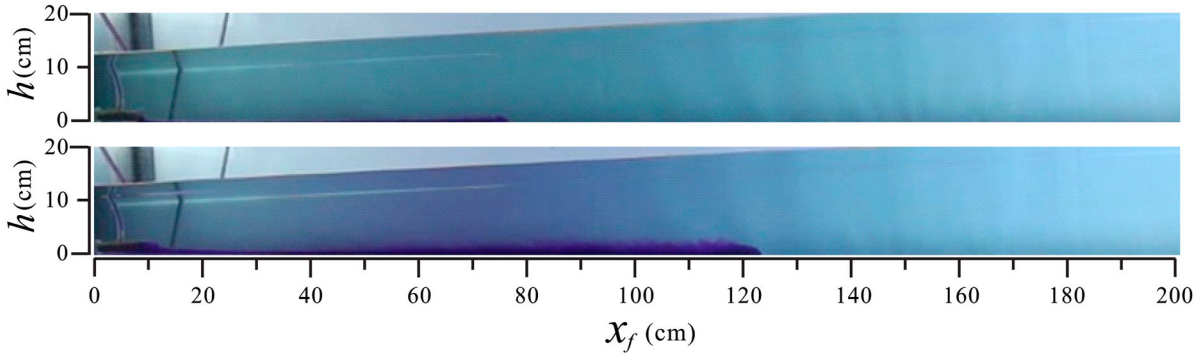

Figure 8 Side-view flow images of gravity currents produced from constant inflow rates at $Q_0 = 0.6\,\mathrm{l\,min^{-1}}$ (equivalent to $10\,\mathrm{cm^3\,s^{-1}}$) (top) and $Q_0 = 3.6\,\mathrm{l\,min^{-1}}$ (equivalent to $60\,\mathrm{cm^3\,s^{-1}}$) (bottom) on a $\theta = 3°$ slope. Distances in the streamwise and wall-normal directions are units of cm with time instances set at $t = 30$ s

4.2 *Gravity currents on milder slopes* $\theta = 3°$ *and* 0°

As shown in Fig. 7, the gravity currents on the slope $\theta = 3°$ and on the horizontal boundary $\theta = 0°$ are closer to a round shape than the gravity currents on slopes $\theta \geq 6°$. Top-view images show that the gravity currents on a horizontal boundary $\theta = 0°$ have a consistent shape from the minimum through maximum volumetric rates. The gravity currents on the slope $\theta = 3°$ have a more elongated shape than the gravity currents on the horizontal boundary $\theta = 0°$ but a shape rounder than the shape on the steeper slopes $\theta \geq 6°$. The side-view images in Fig. 8 show that the gravity currents in the streamwise direction have a more uniform thickness. Figure 9 shows the front velocity histories for the gravity currents on $\theta = 3°$ and $\theta = 0°$. Our results show that the front velocity takes a peak value before decelerating, similar to the gravity currents on $\theta \geq 6°$.

4.3 *Dimensional analysis*

As per previous explanation, the study followed a more fundamental principle in describing the characteristics of the gravity currents produced from a constant inflow on unbounded uniform slopes, employing five dimensionless parameters, from π_1 to π_5, as defined in Section 2. The values of the five parameters were determined based on regression from measurements of density, and the geometric and kinematic features of the gravity currents with temporal and spatial variations once the currents approach

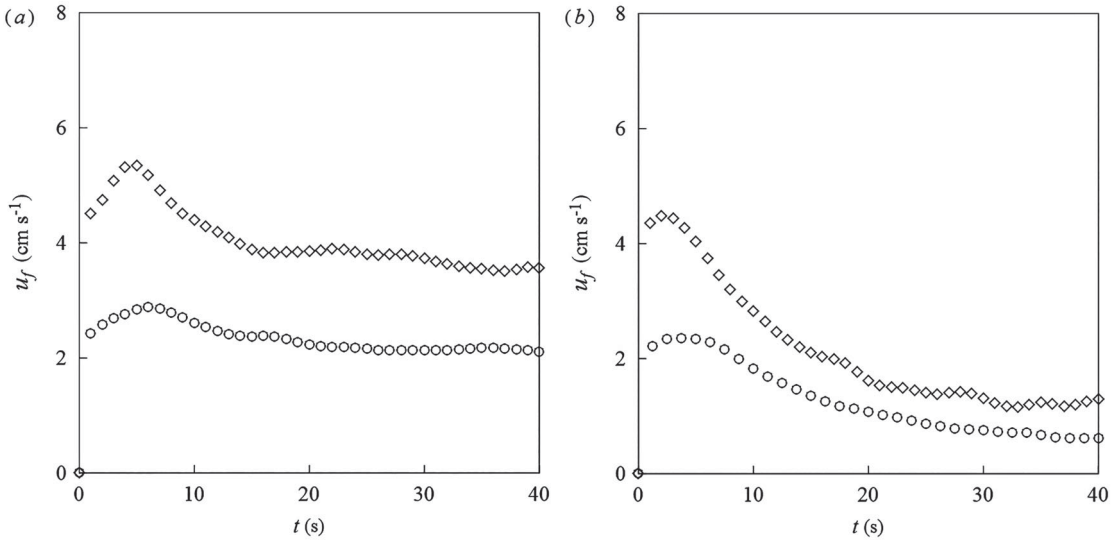

Figure 9 Front velocity histories for the gravity currents produced from constant inflow rates at $Q_0 = 0.61\,\mathrm{min}^{-1}$ (equivalent to $10\,\mathrm{cm}^3\,\mathrm{s}^{-1}$) (°) and $3.61\,\mathrm{min}^{-1}$ (equivalent to $60\,\mathrm{cm}^3\,\mathrm{s}^{-1}$) (◇), on unbounded uniform slopes; (a) $\theta = 3^\circ$ and (b) $\theta = 0^\circ$

Table 2 Experimental parameters for the gravity currents produced from a constant inflow on unbounded uniform slopes, including the maximum width, maximum front velocity and dimensionless parameters from π_1 to π_5

Experiment	$b_{\max}$ (cm)	$u_f^{\max}$ (cm s^{-1})	π_1	π_2	π_3	π_4	π_5
A1	$56.03^{+0.19}_{-0.19}$	$2.36^{+0.07}_{-0.09}$	$0.965^{+0.014}_{-0.020}$	–	$1.083^{+0.041}_{-0.054}$	$0.891^{+0.049}_{-0.026}$	$0.147^{+0.006}_{-0.005}$
A2	$72.22^{+0.60}_{-0.86}$	$3.68^{+0.19}_{-0.25}$	$1.011^{+0.033}_{-0.042}$	–	$0.955^{+0.068}_{-0.066}$	$1.082^{+0.058}_{-0.092}$	$0.154^{+0.023}_{-0.021}$
A3	$99.81^{+0.76}_{-0.52}$	$4.49^{+0.09}_{-0.14}$	$1.127^{+0.004}_{-0.003}$	–	$1.098^{+0.059}_{-0.094}$	$1.081^{+0.097}_{-0.060}$	$0.126^{+0.018}_{-0.011}$
A4	$118.53^{+0.65}_{-0.98}$	$4.83^{+0.11}_{-0.07}$	$1.157^{+0.014}_{-0.015}$	–	$0.979^{+0.033}_{-0.021}$	$1.245^{+0.050}_{-0.063}$	$0.123^{+0.009}_{-0.008}$
B1	$48.54^{+1.75}_{-1.19}$	$2.89^{+0.22}_{-0.10}$	$0.389^{+0.016}_{-0.014}$	$0.009^{+0.001}_{-0.002}$	$0.572^{+0.022}_{-0.014}$	$0.496^{+0.009}_{-0.011}$	$0.021^{+0.003}_{-0.003}$
B2	$59.65^{+3.37}_{-4.79}$	$3.83^{+0.32}_{-0.32}$	$0.394^{+0.019}_{-0.039}$	$0.010^{+0.002}_{-0.001}$	$0.540^{+0.010}_{-0.018}$	$0.535^{+0.026}_{-0.051}$	$0.022^{+0.005}_{-0.003}$
B3	$90.12^{+0.98}_{-1.63}$	$4.74^{+0.13}_{-0.07}$	$0.424^{+0.042}_{-0.043}$	$0.012^{+0.001}_{-0.001}$	$0.478^{+0.022}_{-0.022}$	$0.669^{+0.055}_{-0.062}$	$0.025^{+0.002}_{-0.002}$
B4	$110.26^{+2.72}_{-3.81}$	$5.34^{+0.33}_{-0.33}$	$0.477^{+0.041}_{-0.034}$	$0.013^{+0.001}_{-0.001}$	$0.481^{+0.036}_{-0.024}$	$0.774^{+0.031}_{-0.034}$	$0.028^{+0.002}_{-0.003}$
C1	$47.69^{+0.53}_{-1.19}$	$3.69^{+0.19}_{-0.11}$	$0.272^{+0.021}_{-0.027}$	$0.016^{+0.001}_{-0.003}$	$0.340^{+0.008}_{-0.004}$	$0.520^{+0.038}_{-0.057}$	$0.020^{+0.001}_{-0.001}$
C2	$58.83^{+3.37}_{-4.79}$	$4.72^{+0.32}_{-0.42}$	$0.304^{+0.009}_{-0.009}$	$0.017^{+0.001}_{-0.001}$	$0.340^{+0.008}_{-0.005}$	$0.603^{+0.028}_{-0.017}$	$0.019^{+0.003}_{-0.002}$
C3	$81.12^{+1.59}_{-0.96}$	$5.65^{+0.17}_{-0.14}$	$0.319^{+0.020}_{-0.029}$	$0.020^{+0.001}_{-0.001}$	$0.305^{+0.016}_{-0.016}$	$0.714^{+0.059}_{-0.048}$	$0.020^{+0.003}_{-0.005}$
C4	$98.68^{+3.83}_{-3.19}$	$6.04^{+0.45}_{-0.47}$	$0.354^{+0.015}_{-0.011}$	$0.021^{+0.001}_{-0.002}$	$0.330^{+0.022}_{-0.011}$	$0.757^{+0.015}_{-0.010}$	$0.023^{+0.003}_{-0.005}$
D1	$48.41^{+1.84}_{-2.23}$	$4.39^{+0.32}_{-0.19}$	$0.202^{+0.313}_{-0.016}$	$0.018^{+0.002}_{-0.002}$	$0.250^{+0.012}_{-0.007}$	$0.475^{+0.072}_{-0.039}$	$0.020^{+0.003}_{-0.006}$
D2	$62.68^{+1.13}_{-2.52}$	$5.37^{+0.18}_{-0.26}$	$0.218^{+0.052}_{-0.036}$	$0.020^{+0.003}_{-0.004}$	$0.263^{+0.018}_{-0.022}$	$0.502^{+0.122}_{-0.119}$	$0.024^{+0.006}_{-0.005}$
D3	$83.78^{+0.92}_{-0.63}$	$6.13^{+0.13}_{-0.08}$	$0.300^{+0.012}_{-0.020}$	$0.021^{+0.002}_{-0.001}$	$0.277^{+0.014}_{-0.024}$	$0.728^{+0.009}_{-0.008}$	$0.022^{+0.003}_{-0.005}$
D4	$101.31^{+1.68}_{-2.10}$	$6.67^{+0.23}_{-0.39}$	$0.341^{+0.031}_{-0.019}$	$0.021^{+0.002}_{-0.001}$	$0.305^{+0.020}_{-0.019}$	$0.784^{+0.042}_{-0.030}$	$0.025^{+0.007}_{-0.008}$
E1	$49.75^{+1.45}_{-2.04}$	$5.06^{+0.20}_{-0.34}$	$0.261^{+0.012}_{-0.019}$	$0.020^{+0.001}_{-0.001}$	$0.258^{+0.005}_{-0.005}$	$0.649^{+0.037}_{-0.054}$	$0.019^{+0.001}_{-0.003}$
E2	$68.12^{+4.23}_{-4.50}$	$5.96^{+0.41}_{-0.47}$	$0.315^{+0.004}_{-0.003}$	$0.021^{+0.004}_{-0.002}$	$0.272^{+0.006}_{-0.008}$	$0.791^{+0.011}_{-0.017}$	$0.023^{+0.004}_{-0.004}$
E3	$86.19^{+3.81}_{-5.33}$	$6.68^{+0.31}_{-0.42}$	$0.330^{+0.027}_{-0.030}$	$0.022^{+0.001}_{-0.002}$	$0.271^{+0.011}_{-0.017}$	$0.841^{+0.075}_{-0.053}$	$0.025^{+0.001}_{-0.001}$
E4	$101.62^{+2.09}_{-1.91}$	$6.78^{+0.17}_{-0.21}$	$0.352^{+0.038}_{-0.022}$	$0.023^{+0.002}_{-0.001}$	$0.296^{+0.029}_{-0.032}$	$0.829^{+0.056}_{-0.067}$	$0.025^{+0.003}_{-0.004}$
F1	$50.10^{+1.56}_{-0.94}$	$5.27^{+0.19}_{-0.07}$	$0.243^{+0.005}_{-0.011}$	$0.020^{+0.003}_{-0.002}$	$0.251^{+0.013}_{-0.014}$	$0.602^{+0.013}_{-0.013}$	$0.020^{+0.005}_{-0.005}$
F2	$68.86^{+1.53}_{-1.85}$	$6.11^{+0.29}_{-0.21}$	$0.291^{+0.008}_{-0.008}$	$0.021^{+0.004}_{-0.002}$	$0.262^{+0.004}_{-0.006}$	$0.736^{+0.048}_{-0.035}$	$0.024^{+0.001}_{-0.002}$
F3	$87.03^{+1.34}_{-1.45}$	$6.81^{+0.13}_{-0.18}$	$0.306^{+0.023}_{-0.032}$	$0.023^{+0.001}_{-0.001}$	$0.260^{+0.006}_{-0.007}$	$0.798^{+0.058}_{-0.110}$	$0.029^{+0.006}_{-0.005}$
F4	$102.51^{+1.39}_{-2.35}$	$7.05^{+0.16}_{-0.24}$	$0.345^{+0.024}_{-0.028}$	$0.024^{+0.002}_{-0.001}$	$0.297^{+0.017}_{-0.022}$	$0.832^{+0.062}_{-0.042}$	$0.032^{+0.003}_{-0.003}$

Note: Error estimates are added to or subtracted from the maximum and minimum values.

a quasi-equilibrium state. The five parameters are functions of the inlet Reynolds number and the slope angle and are quantified in order as in the following (Table 2).

Figure 10 shows gravity current shapes, defined as the ratio between the maximum width $b_{\max}$ and the front location measured from the virtual origin $x_{f,v}$, i.e. $\pi_1 = b_{\max} x_{f,v}^{-1}$. The

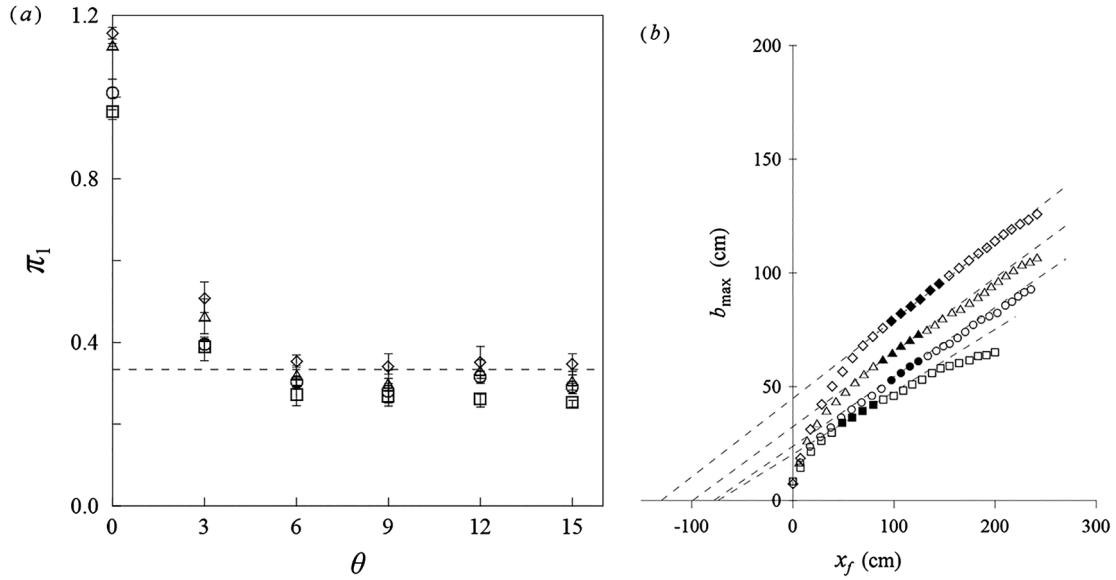

Figure 10 Dimensionless parameter π_1 versus slope angle θ at different volumetric inflow rates. Symbols: ◇: $Q_0 = 3.6$, Δ: $Q_0 = 2.4$, °: $Q_0 = 1.2$ and □: $Q_0 = 0.6\,\mathrm{l\,min^{-1}}$. The parameters are determined by linear regression. The illustrated case on the right side refers to $\theta = 6°$. Solid symbols denote the time duration for gravity currents in a quasi-steady state. Dashed line in the left side figure represents the empirical estimate given by Hauenstein and Dracos (1984)

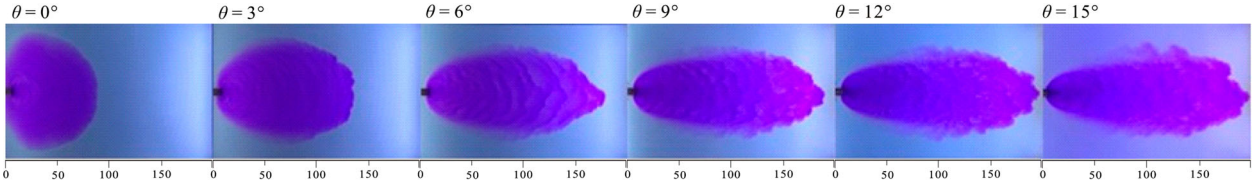

Figure 11 Comparison of the flow morphologies of gravity currents on unbounded uniform slopes. Corresponding to images from left to right, $\theta = 0°$, 3°, 6°, 9°, 12° and 15°. The volumetric inflow rate is at $Q_0 = 3.6\,\mathrm{l\,min^{-1}}$ (equivalent to $60\,\mathrm{cm^3\,s^{-1}}$), with time instances set at $t = 40\,\mathrm{s}$

location of the virtual origin is defined with the regression of $x_{f,v} \sim b_{max}$, as shown in Fig. 10. From the empirical relationships, i.e. Eqs (1) and (2), $\cos\theta/C_6 = b_{max}x_{f,v}^{-1}$, it is known that the dimensionless parameter π_1 is related to $\cos\theta/C_6$. Figure 10 shows the results from the gravity currents on $\theta = 6°$ as an example.

Large values of π_1 indicate that the gravity currents have a round shape while small values of π_1 indicate that the gravity currents have an elongated shape. Figure 10 shows that π_1 ranges from 0.2 to 0.4 as $\theta \geq 6°$, regardless of the change in volumetric inflow rate. The results are consistent with the experimental images displayed in Fig. 11. For the gravity currents on the slope $\theta = 3°$ and on the horizontal boundary $\theta = 0°$, the values are about 0.45 and 1.0, respectively. As shown in Fig. 10, shape factor π_1 approaches 0.33 as $\theta \geq 6°$. Figure 12 shows the shape factor π_2 of the gravity currents, defined as the ratio of head height h and the front location from virtual origin $x_{f,v}$, i.e. $\pi_2 = hx_{f,v}^{-1}$. The head height is the maximum value measured at each instant from the bulbous-like front (Nogueira et al., 2014). Figure 12 shows that π_2 values are larger for the gravity currents on $\theta \geq 6°$ than those for the gravity currents on the slope $\theta = 3°$. Dimensionless parameter π_2 approaches 0.02 as $\theta \geq 9°$. It is noted that the thickness of gravity currents on the horizontal boundary is so small that the increase in proportion to distance cannot be measured accurately.

Figure 13 shows the relationship between the front location, buoyancy flux, and time in dimensionless parameter $\pi_3 = W_p^{1/3}x_{f,v}^{-4/3}t$. According to Hauenstein and Dracos (1984), it is known that $x_{v,f} = (1.11C_6/\cos\theta)W_p^{1/4}t^{3/4}$, suggesting that $\pi_3 = (1.11C_6/\cos\theta)^{-4/3}$. Our experimental data show that the dimensionless parameter π_3 can be measured from the slope of the $x_{f,v}^{4/3}$ versus t plot. It is found that dimensionless parameter π_3 decreases as the slope angle increases. For the gravity currents on the steeper slopes $\theta \geq 6°$, the values of π_3 are close to 0.3. It is noted that the value inferred from the empirical relationship in Hauenstein and Dracos (1984) stands at around 0.201, regardless of the slope angle. Figure 14 shows the relationship between the maximum width, buoyancy flux, and time in dimensionless parameter $\pi_4 = W_p^{-1/3}b_{max}^{4/3}t$. According to our experimental data, dimensionless parameter π_4 can be measured from the slope of the $b_{max}^{4/3}$ versus t plot. In Fig. 14, except for the gravity currents on the horizontal boundary $\theta = 0°$, dimensionless parameter π_4 approaches 0.6 as $\theta \geq 3°$.

As per previous explanation, the study also examined fluid density in the head of gravity currents, with the density difference being expected to decrease, due to turbulent entrainment as the gravity currents propagate downslope. The relationship

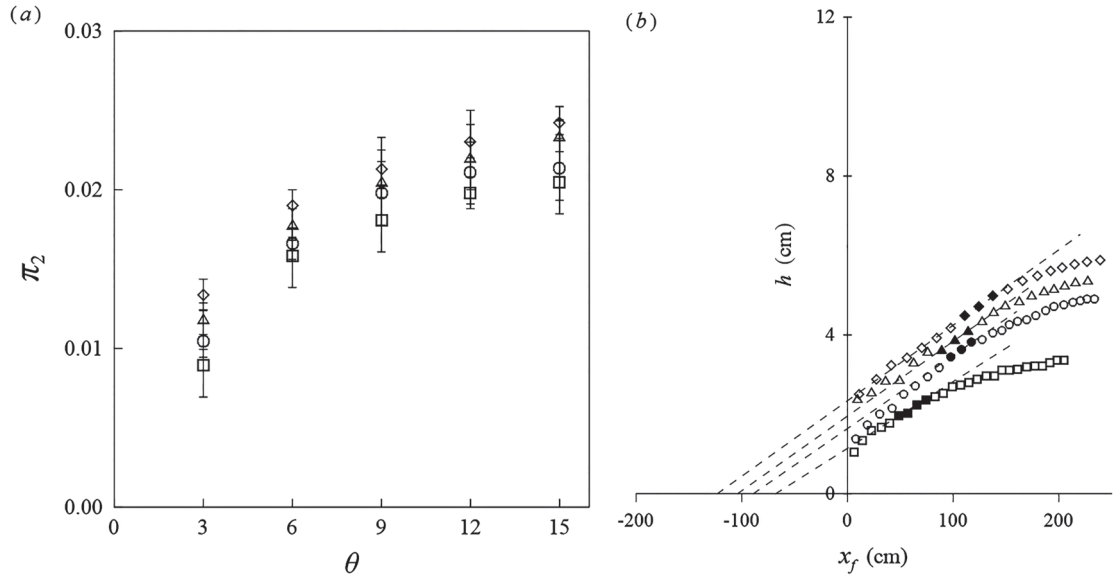

Figure 12 Dimensionless parameter π_2 versus slope angle θ at different volumetric inflow rates. Symbols: ◇: $Q_0 = 3.6$, Δ: $Q_0 = 2.4$, °: $Q_0 = 1.2$ and □: $Q_0 = 0.61\,\mathrm{min}^{-1}$. The parameters are determined by linear regression. The illustrated case on the right side refers to $\theta = 6°$. Solid symbols denote the time duration for gravity currents in a quasi-steady state

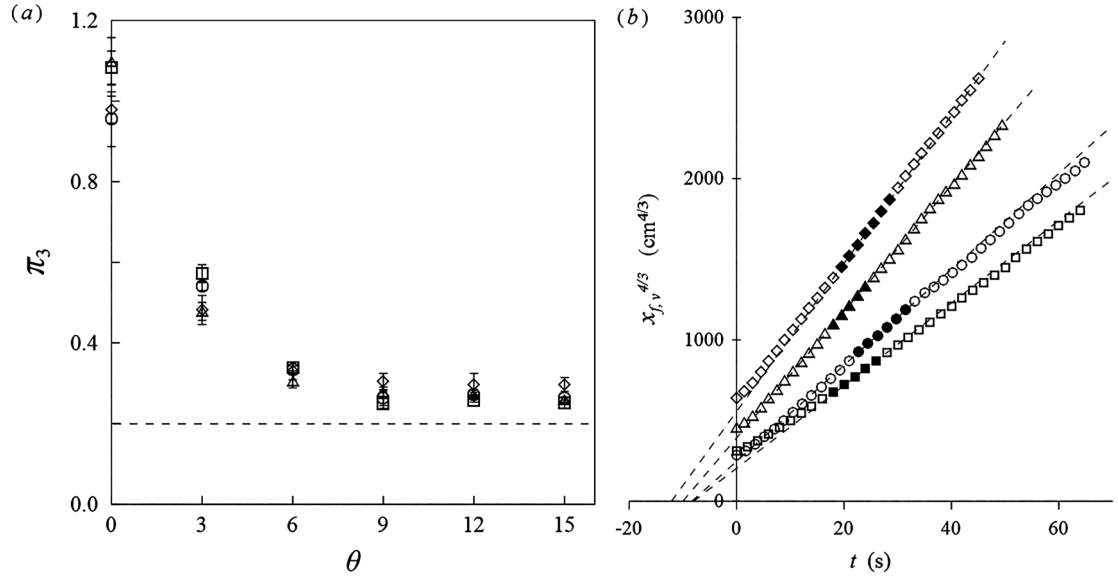

Figure 13 Dimensionless parameter π_3 versus slope angle θ at different volumetric inflow rates. Symbols: ◇: $Q_0 = 3.6$, Δ: $Q_0 = 2.4$, °: $Q_0 = 1.2$ and □: $Q_0 = 0.61\,\mathrm{min}^{-1}$. The parameters are determined by linear regression. The illustrated case on the right side refers to $\theta = 6°$. Solid symbols denote the time duration for gravity currents in a quasi-steady state. Dashed line in the left side figure represents the empirical estimate given by Hauenstein and Dracos (1984)

between fluid density in the head, buoyancy flux, and front location is defined in the dimensionless parameter $\pi_5 = W_p^{-2/3} x_{f,v}^{5/3} (\Delta\rho_f / \rho_0) g$. According to our experimental data, dimensionless parameter π_5 can be measured from the slope of the $(\Delta\rho_f / \rho_0)^{-3/5}$ versus x_f plot. In Fig. 15a, π_5 value is largely independent of the variation of Q_0. In line with the explanation in Fig. 6a, oscillations in the front velocity are apparent for the gravity currents on the steeper slopes. In such a situation, the oscillations in the front velocity may cause errors in measurement of density in the current head with a syringe. However, all the dimensionless values converge and fall within a reasonable range of errors. Except for the gravity currents on the horizontal boundary $\theta = 0°$, dimensionless parameter π_5 approaches 0.02.

Dimensional analysis shows that the gravity currents behave in a similar fashion for $\theta \geq 6°$. The five dimensionless parameters, from π_1 to π_5, show that the influence of the inlet Reynolds number is small provided that the inlet Reynolds number is

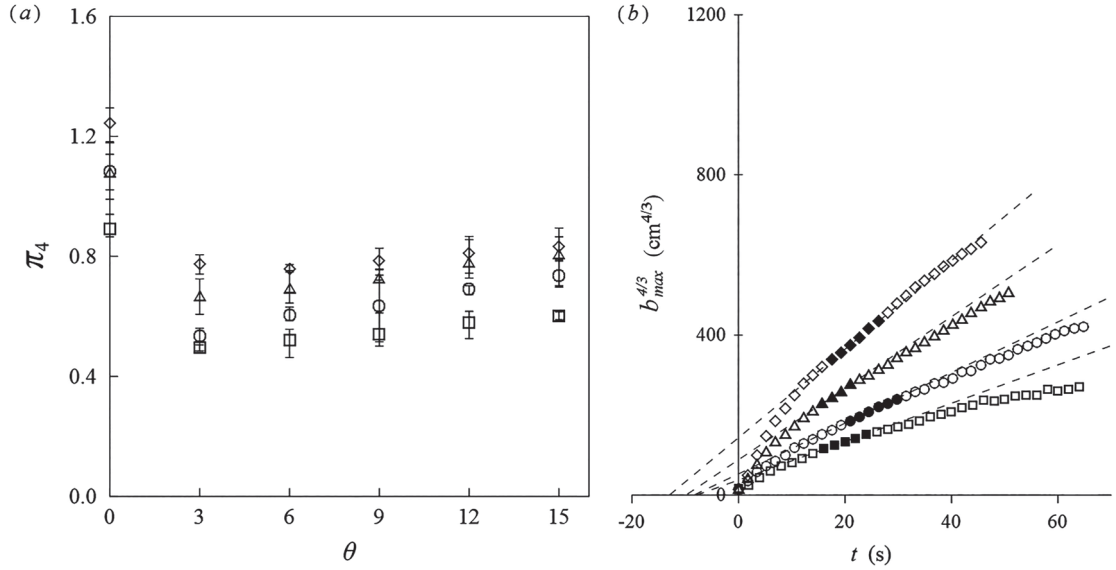

Figure 14 Dimensionless parameter π_4 versus slope angle θ at different volumetric inflow rates. Symbols: ◇: $Q_0 = 3.6$, Δ: $Q_0 = 2.4$, °: $Q_0 = 1.2$ and □: $Q_0 = 0.6\,\mathrm{l\,min^{-1}}$. The parameters are determined by linear regression. The illustrated case on the right side refers to $\theta = 6°$. Solid symbols denote the time duration for gravity currents in a quasi-steady state

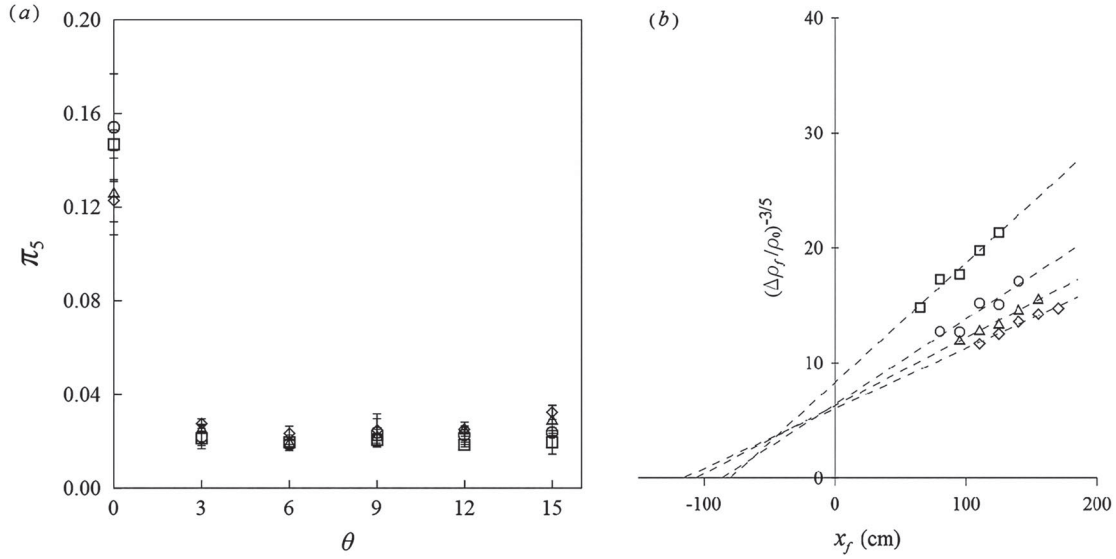

Figure 15 Dimensionless parameter π_5 versus slope angle θ at different volumetric inflow rates. Symbols: ◇: $Q_0 = 3.6$, Δ: $Q_0 = 2.4$, °: $Q_0 = 1.2$ and □: $Q_0 = 0.6\,\mathrm{l\,min^{-1}}$. The parameters are determined by linear regression. The illustrated case on the right side refers to $\theta = 6°$. Solid symbols denote the time duration for gravity currents in a quasi-steady state

sufficiently large. By comparison, the gravity currents on $\theta \leq 3°$ tend to be more influenced by the inlet Reynolds number and the slope angle. Simpson (1997) reported that the viscous effects become unimportant when the Reynolds numbers exceed 1000. The study finds that for sufficiently large inlet Reynolds numbers, the gravity currents in our experiments seem to approach the regime of Reynolds number independence. In this case, the development of gravity currents is dependent on the slope angle and weakly dependent on the inlet Reynolds number. Results from our experiments are consequently expected to be applicable to larger scale natural or man-made environments.

5 Conclusions

In this study we conducted experiments to investigate the gravity currents produced from a constant inflow on unbounded uniform slopes. The inlet Reynolds number and the slope angle were varied systematically in the experiments. We employed the dimensional analysis, with five dimensionless parameters, to describe the characteristics of the gravity currents on steeper and milder slopes. In the experiments, top-view images show that gravity currents have a rounder shape on milder slopes of $\theta \leq 3°$, compared with a more elongated shape on steeper slopes of $\theta \geq 6°$. As the volumetric inflow rate increases, in line with

the inlet Reynolds number, flow similarities are expected when the inlet Reynolds number is sufficiently large. Simpson (1997) reported that the viscous effects become unimportant when the Reynolds numbers exceed 1000. The dimensional analysis shows that for sufficiently large inlet Reynolds numbers, the gravity currents in our experiments seem to approach the regime of Reynolds number independence. Therefore, results from our experiments are expected to be applicable to larger scale natural or man-made environments.

One of the limitations in this study is the influence of density difference between the inflow heavy fluid and light ambient fluid, as the density difference was maintained unchanged in the experiments. According to our previous studies (Dai & Huang, 2020, 2021), with a surge-type buoyancy source, the density difference between the heavy fluid and ambient fluid does not change the flow pattern qualitatively but the parameters describing the gravity currents may be subject to change quantitatively as the density difference is varied. For the gravity currents produced from a constant inflow, the influence of density difference between the heavy fluid and ambient fluid is still unknown and awaits further investigation.

Acknowledgments

The authors would like to thank Mr L.-C. Hsu and Mr Y.-A. Li for help in running the experiments.

Disclosure statement

No potential conflict of interest was reported by the author(s).

Funding

The research was funded by National Taiwan University through grants 106R7739, 106R7830, 107L7830, 107L7734, 112L7826 and by Taiwan National Science and Technology Council through grants 107-2221-E-197-009, 108-2221-E-197-001-MY2, 111-2221-E-002-113-MY3.

Notation

$b_{\max}$ = maximum width of spreading gravity currents (cm)
b_0 = width of diffuser (cm)
h = maximum head height (cm)
h_0 = height of diffuser (cm)
g = gravitational acceleration (cm s^{-2})
g' = reduced gravity (cm s^{-2})
Q_0 = volumetric inflow rate (cm^3 s^{-1})
Re = Reynolds number (–)
t = time (s)
u_f = front velocity of gravity currents (cm s^{-1})
W_p = buoyancy flux (cm^4 s^{-3})
x_f = front location (cm)
$x_{f,v}$ = distance between the virtual origin and the front (cm)
ν = kinematic viscosity of fluid (cm^2 s^{-1})
π_1 = shape factor of the gravity currents in the spanwise direction (–)
π_2 = shape factor of the gravity currents in the wall-normal direction (–)
π_3 = dimensionless parameter relating front location and time (–)
π_4 = dimensionless parameter relating maximum width and time (–)
π_5 = dimensionless parameter relating the density difference in the head and front location (–)
ρ_0 = density of ambient fluid (g cm^{-3})
ρ_1 = density of inflow heavy fluid (g cm^{-3})
θ = slope angle (–)
$\Delta\rho$ = density excess of inflow heavy fluid (g cm^{-3})
$\Delta\rho_f$ = density excess of the fluid in the head of the gravity currents (g cm^{-3})

References

Adduce, C., Maggi, M. R., & De Falco, M. C. (2022). Non-intrusive density measurements in gravity currents interacting with an obstacle. *Acta Geophysica*, *70*(5), 2499–2510. https://doi.org/10.1007/s11600-021-00709-z

Adduce, C., Sciortino, G., & Proietti, S. (2012). Gravity currents produced by lock exchanges: Experiments and simulations with a two-layer shallow-water model with entrainment. *Journal of Hydraulic Engineering*, *138*(2), 111–121. https://doi.org/10.1061/(ASCE)HY.1943-7900.0000484

Alavian, V. (1986). Behavior of density currents on an incline. *Journal of Hydraulic Engineering*, *112*(1), 27–42. https://doi.org/10.1061/(ASCE)0733-9429(1986)112:1(27)

Allen, J. (1985). *Principles of physical sedimentology*. Allen & Unwin.

Baines, P. G. (2001). Mixing in flows down gentle slopes into stratified environments. *Journal of Fluid Mechanics*, *443*, 237–270. https://doi.org/10.1017/S0022112001005250

Bonnecaze, R. T., & Lister, J. R. (1999). Particle-driven gravity currents down planar slopes. *Journal of Fluid Mechanics*, *390*, 75–91. https://doi.org/10.1017/S0022112099004917

Borden, Z., & Meiburg, E. (2013). Circulation based models for Boussinesq gravity currents. *Physics of Fluids*, *25*(10), Article 101301. https://doi.org/10.1063/1.4825035

Britter, R. E., & Linden, P. F. (1980). The motion of the front of a gravity current travelling down an incline. *Journal of Fluid Mechanics*, *99*(3), 531–543. https://doi.org/10.1017/S0022112080000754

Cantero, M. I., Lee, J. R., Balachandar, S., & Garcia, M. H. (2007). On the front velocity of gravity currents. *Journal of Fluid Mechanics*, *586*, 1–39. https://doi.org/10.1017/S0022112007005769

Chawdhary, S., Khosronejad, A., Christodoulou, G., & Sotiropoulos, F. (2018). Large eddy simulation of density current on sloping beds. *International Journal of Heat and Mass Transfer*, *120*, 1374–1385. https://doi.org/10.1016/j.ijheatmasstransfer.2017.12.063

Dai, A. (2013a). Experiments on gravity currents propagating on different bottom slopes. *Journal of Fluid Mechanics*, *731*, 117–141. https://doi.org/10.1017/jfm.2013.372

Dai, A. (2013b). Gravity currents propagating on sloping boundaries. *Journal of Hydraulic Engineering*, *139*(6), 593–601. https://doi.org/10.1061/(ASCE)HY.1943-7900.0000716

Dai, A. (2014). Non-Boussinesq gravity currents propagating on different bottom slopes. *Journal of Fluid Mechanics*, *741*, 658–680. https://doi.org/10.1017/jfm.2014.5

Dai, A., & Garcia, M. H. (2010). Gravity currents down a slope in deceleration phase. *Dynamics of Atmospheres and Oceans*, *49*(1), 75–82. https://doi.org/10.1016/j.dynatmoce.2008.11.001

Dai, A., & Huang, Y. L. (2020). Experiments on gravity currents propagating on unbounded uniform slopes. *Environmental Fluid Mechanics*, *20*(6), 1637–1662. https://doi.org/10.1007/s10652-020-09758-2

Dai, A., & Huang, Y. L. (2021). Boussinesq and non-Boussinesq gravity currents propagating on unbounded uniform slopes in the deceleration phase. *Journal of Fluid Mechanics*, *917*, Article A23. https://doi.org/10.1017/jfm.2021.300

Dai, A., Ozdemir, C. E., Cantero, M. I., & Balachandar, S. (2012). Gravity currents from instantaneous sources down a slope. *Journal of Hydraulic Engineering*, *138*(3), 237–246. https://doi.org/10.1061/(ASCE)HY.1943-7900.0000500

Fannelop, T. K. (1994). *Fluid mechanics for industrial safety and environmental protection*. Elsevier.

Hauenstein, W., & Dracos, T. (1984). Investigation of plunging density currents generated by inflows in lake. *Journal of Hydraulic Research*, *22*(3), 157–179. https://doi.org/10.1080/00221688409499404

Hopfinger, E. J. (1983). Snow avalanche motion and related phenomena. *Annual Review of Fluid Mechanics*, *15*(1), 47–76. https://doi.org/10.1146/fluid.1983.15.issue-1

Huppert, H. E. (2006). Gravity currents: A personal perspective. *Journal of Fluid Mechanics*, *554*, 299–322. https://doi.org/10.1017/S002211200600930X

Huppert, H. E., & Simpson, J. E. (1980). The slumping of gravity currents. *Journal of Fluid Mechanics*, *99*(4), 785–799. https://doi.org/10.1017/S0022112080000894

La Rocca, M., Adduce, C., Sciortino, G., & Pinzon, A. B. (2008). Experimental and numerical simulation of three-dimensional gravity currents on smooth and rough bottom. *Physics of Fluids*, *20*(10), Article 106603. https://doi.org/10.1063/1.3002381

Maggi, M. R., Adduce, C., & Negretti, M. E. (2022). Lock-release gravity currents propagating over roughness elements. *Environmental Fluid Mechanics*, *22*(2–3), 383–402. https://doi.org/10.1007/s10652-022-09845-6

Marino, B. M., Thomas, L. P., & Linden, P. F. (2005). The front condition for gravity currents. *Journal of Fluid Mechanics*, *536*, 49–78. https://doi.org/10.1017/S0022112005004933

Martin, A., Negretti, M. E., & Hopfinger, E. J. (2019). Development of gravity currents on slopes under different interfacial instability conditions. *Journal of Fluid Mechanics*, *880*, 180–208. https://doi.org/10.1017/jfm.2019.713

Maxworthy, T. (2010). Experiments on gravity currents propagating down slopes. Part 2. The evolution of a fixed volume of fluid released from closed locks into a long, open channel. *Journal of Fluid Mechanics*, *647*, 27–51. https://doi.org/10.1017/S0022112009006065

Negretti, M. E., Flòr, J. B., & Hopfinger, E. J. (2017). Development of gravity currents on rapidly changing slopes. *Journal of Fluid Mechanics*, *833*, 70–97. https://doi.org/10.1017/jfm.2017.696

Nogueira, H. I. S., Adduce, C., Alves, E., & Franca, M. J. (2013a). Analysis of lock-exchange gravity currents over smooth and rough beds. *Journal of Hydraulic Research*, *51*(4), 417–431. https://doi.org/10.1080/00221686.2013.798363

Nogueira, H. I. S., Adduce, C., Alves, E., & Franca, M. J. (2013b). Image analysis technique applied to lock-exchange gravity currents. *Measurement Science and Technology*, *24*(4), Article 047001. https://doi.org/10.1088/0957-0233/24/4/047001

Nogueira, H. I. S., Adduce, C., Alves, E., & Franca, M. J. (2014). Dynamics of the head of gravity currents. *Environmental Fluid Mechanics*, *14*(2), 519–540. https://doi.org/10.1007/s10652-013-9315-2

Ross, A. N., Linden, P. F., & Dalziel, S. B. (2002). A study of three-dimensional gravity currents on a uniform slope. *Journal of Fluid Mechanics*, *453*, 239–261. https://doi.org/10.1017/S0022112001006899

Shin, J. O., Dalziel, S. B., & Linden, P. F. (2004). Gravity currents produced by lock exchange. *Journal of Fluid Mechanics*, *521*, 1–34. https://doi.org/10.1017/S002211200400165X

Simpson, J. E. (1997). *Gravity currents* (2nd ed.). Cambridge University Press.

Ungarish, M. (2009). *An introduction to gravity currents and intrusions*. Chapman and Hall/CRC.

Ungarish, M., & Hogg, A. J. (2018). Models of internal jumps and the fronts of gravity currents: Unifying two-layer theories and deriving new results. *Journal of Fluid Mechanics*, *846*, 654–685. https://doi.org/10.1017/jfm.2018.219

Wu, C. S., & Dai, A. (2020). Experiments on two-layer stratified gravity currents in the slumping phase. *Journal of Hydraulic Research*, *58*(5), 831–844. https://doi.org/10.1080/00221686.2019.1671517